European Review for Medical and Pharmacological Sciences 2022; 26: 8376-8394

Role of machine learning algorithms in predicting the treatment outcome of uterine fibroids using high-intensity focused ultrasound ablation with an immediate nonperfused volume ratio of at least 90%

E. AKPINAR[1,2], O.-C BAYRAK[2], C. NADARAJAN[3,4], M.-H. MÜSLÜMANOĞLU[5], M.-D. NGUYEN[6], B. KESERCI[2,3,4]

[1]Department of Physics, [2]Intelligent Healthcare Innovation Research Center, Yildiz Technical University, Istanbul, Turkey
[3]Department of Radiology, School of Medical Sciences, Universiti Sains Malaysia, Kelantan, Malaysia
[4]Department of Radiology, Hospital Universiti Sains Malaysia, Kubang Kerian, Kelantan, Malaysia
[5]Department of Molecular Biology and Genetics, Faculty of Arts and Science, Yildiz Technical University, Istanbul, Turkey
[6]Department of Radiology, Pham Ngoc Thach University of Medicine, Ho Chi Minh City, Vietnam

Abstract. – OBJECTIVE: This study aimed to investigate the role of machine learning (ML) classifiers to determine the most informative multiparametric (mp) magnetic resonance imaging (MRI) features in predicting the treatment outcome of high-intensity focused ultrasound (HIFU) ablation with an immediate nonperfused volume (NPV) ratio of at least 90%.

PATIENTS AND METHODS: Seventy-three women who underwent HIFU treatment were divided into groups A (n=47) and B (n=26), comprising patients with an NPV ratio of at least 90% and <90%, respectively. An ensemble feature ranking model was introduced based on the score values assigned to the features by five different ML classifiers to determine the most informative mpMRI features. The relationship between the mpMRI features and the immediate NPV ratio of 90% was evaluated using Pearson's correlation coefficients. The diagnostic ability of the ML classifiers was evaluated using standard performance metrics, including the area under the receiver operating characteristic curve, accuracy, sensitivity, and specificity in eight folds cross-validation.

RESULTS: For all the 12 most informative features, the area under receiver operating characteristic curve (AUROC), accuracy, specificity, and sensitivity ranged from 0.5 to 0.97, 0.34 to 0.97, 0.56 to 1.0, and 0.87 to 1.0, respectively. The gradient boosting (GBM) classifier demonstrated the best predictive performance with an AUROC of 0.95 and accuracy of 0.92, followed by the random forest, AdaBoost, logistic regression, and support vector classifiers, which yielded an AUROC of 0.92, 0.92, 0.83, and 0.78 and accuracy of 0.96, 0.88, 0.84, and 0.84, respectively. GBM had the best classifier performance with the best performing features from each mpMRI group, K^{trans} ratio of the fibroid to the myometrium, the ratio of area under the curve of the fibroid to the myometrium, subcutaneous fat thickness, the ratio of apparent diffusion coefficient value of fibroid to the myometrium, and T2-signal intensity of the fibroid.

CONCLUSIONS: The preliminary findings of this study suggest that the most informative and best performing features from each mpMRI group should be considered for predicting the treatment outcome of HIFU ablation to achieve an immediate NPV ratio of 90%.

Key Words:
High-intensity focused ultrasound, Machine learning, Magnetic resonance imaging, Multiparametric magnetic resonance imaging, Therapeutic outcome, Uterine fibroids.

Introduction

Uterine fibroids, arising from the myometrium and composed of smooth muscle cells, are

Corresponding Authors: Bilgin Keserci, Ph.D; e-mail: bushido.keserci@gmail.com
Nguyen Minh Duc, MD; e-mail: bsnguyenminhduc@pnt.edu.vn

the most common benign tumors of the uterus occurring in approximately 60% and 50% of the women in the reproductive age group and women aged 50 years, respectively[1-4]. Some common symptoms associated with uterine leiomyomas affecting a woman's health and quality of life are pelvic pain, heavy menstrual bleeding, increased frequency of urination, infertility, and recurrent pregnancy loss.

Hysterectomy and myomectomy remain the definitive surgical treatment for uterine fibroids. However, minimally invasive procedures have emerged as conservative approaches for maintaining fertility and preserving women's uteri. Magnetic resonance imaging (MRI)-guided high-intensity focused ultrasound (HIFU) plays an important clinical role in the treatment of uterine fibroids, with abundant evidence available on its safety and efficacy over the last decades[5-31]. MRI functions as an imaging application not only for target volume identification but also for intra-procedural assessment via quantitative temperature mapping and post-treatment assessment. Meanwhile, HIFU acts as a therapeutic application to thermally ablate tissues by producing controlled volumes of thermal coagulation, inducing targeted necrosis deep within the body while sparing the surrounding normal tissues.

Knowledge of the disease pathogenesis and pathophysiology is crucial when practicing holistic but individualized treatments. A literature review indicates that the histopathology of uterine diseases varies among patients. The treatment response varies based on the tissue characteristics, especially its cellularity, diffusivity, and vascularity. Over the past two decades, several studies have evaluated the clinical outcomes of HIFU ablation in the treatment of uterine fibroids based on (1) T2-weighted (T2W) signal intensity (SI) of uterine fibroids, which is the primary MRI feature for the assessment of tissue cellularity[5-17], (2) apparent diffusion coefficient (ADC) maps derived from diffusion-weighted (DW) MRI for the assessment of diffusivity characteristics of the tissues[18-21], and (3) perfusion MR features for the assessment of tissue vascularity[22-31]. However, assessment of the tissue characteristics based on either of the above parameters individually becomes a major limiting factor for accurate differentiation of fibroid and assessment of the treatment's suitability and efficacy. Therefore, accurate analysis of the disease characteristics that influence treatment responsiveness should be performed using a combination of multiparametric (mp) MRI for simultaneous assessment of tissue cellularity, diffusivity, and vascularity. This is critical for understanding the suitability of treatment and predicting the effectiveness of HIFU using MRI guidance.

Well-informed medical decisions require understanding comprehensive information supported by higher scientific accuracy data. This can be achieved by utilizing artificial intelligence (AI) capabilities, which incorporate wider statistically valid evidence-based predictors and advanced MRI technology. Machine learning (ML) methods, which is a branch of AI, are able to increase the granularity of data analysis, category distinctions, and associated tissue responsiveness information. Such capabilities are particularly relevant and essential for the complete assessment of fibroids and ensuring success of the HIFU procedure. Therefore, this study aimed to comparatively evaluate the role of ML classifiers to determine the most informative anatomical features and tissue characteristics of uterine fibroid, outlining its cellularity, diffusivity, and vascularity in predicting the treatment outcome of HIFU ablation to achieve an immediate nonperfused volume (NPV) ratio of at least 90%.

Patients and Methods

Ethics Statement and Patient Characteristics

The study protocol was designed as a retrospective study in accordance with the 1964 Helsinki declaration. Written informed consent was obtained from each patient before initiation of the HIFU-related procedures.

In our study, 73 women (mean age: 38.84 ± 5.75 years; age range: 22-49 years) underwent HIFU treatment. They were divided into two groups: "group A" comprised patients with an NPV ratio of at least 90% (n=47) and "group B" comprised patients with an NPV ratio of less than 90% (n=26). The inclusion criteria were as follows: (1) women aged >18 years, (2) pre- or peri-menopausal women, (3) those with symptomatic uterine fibroids measuring > 3 cm in diameter, and (4) those who underwent MRI examination pre- or post-HIFU treatment. The exclusion criteria were as follows: (1) women with other endometrial diseases, suspected ma-

lignancy, or other uncontrolled systemic diseases, (2) those who underwent myomectomy previously, (3) those with positive pregnancy test results, (4) those with contraindication for MRI, and (5) those with intolerance to MRI contrast agents.

The conceptual flowchart of the present study is illustrated in Figure 1. Further details are provided in the following sections.

MpMRI Protocol and Feature Extraction

The mpMRI protocol, which combines the anatomic information from the T2W MRI sequence with functional information from DW and dynamic contrast enhancement (DCE) MRI sequences, was performed using a clinical HIFU system (Profound Medical Inc., Toronto, Canada) integrated with a 1.5T MR scanner (Ingenia, Philips, The Netherlands).

First, T2W three-dimensional (3D) turbo spin-echo images were acquired for screening using the following parameters: repetition time (TR)/echo time (TE), 1300/130 ms; flip angle (FA), 90°; slice thickness (ST), 1.25 mm; matrix, 224 ×218; field of view (FOV), 250 × 250 mm; number of slices, 160; acquisition time, 190 s; and sagittal plane. Second, the DW MRI series were additionally performed using a fat-suppressed single-shot spin-echo echo-planar imaging (SE-EPI) sequence with b-values: 0, 200, 400, 600, and 800 s/mm^2. The imaging parameters for screening were: TR/TE, 2,500/65 ms; FA, 90°; ST, 1.25 mm; FOV, matrix, 250 × 250 mm; number of slices, 44; acquisition time, 288 s; axial plane. Third, DCE perfusion MRI was carried out during the screening examination as a routine clinical protocol following intravenous administration of Gd-DO3A-butrol (0.1 mmol/kg of body weight, Gadovist, Bayer Schering Pharma, Germany). The following parameters were used in DCE perfusion MRI: TR/TE, 4.0/2.0 ms; FA, 8°; ST, 5 mm; matrix, 230 × 230; FOV, 116 ×114 mm; acquisition time, 132 s; 50 dynamics (five pre-contrast and subsequent 45 post-contrast were obtained every 3.6 s); and axial plane. Finally, the NPV, the size of the ablated volume of uterine fibroids, was assessed immediately after treatment with contrast-enhanced (CE) MRI based on the following parameters: TR/TE, 5.5/2.7; FA, 10°; inversion recovery (IR) delay, 90 ms; ST, 1.5 mm; matrix, 150 × 150; FOV, 250 × 250 mm; number of slices, 90; acquisition time, 173 seconds; and coronal plane.

MpMRI data extraction was performed manually by screening the MRI data for each patient based on the consensus of two expert radiologists with >10 years of experience in reading pelvic MR images using the IntelliSpace Portal software (version 10.0, Philips) that includes the following dedicated tools: Multimodality viewer, MR T1 Permeability, MR T1 Perfusion, and MR Diffusion. A total of 37 MRI features, which combine the anatomical and different tissue characteristics based on cellularity, vascularity, and diffusivity were considered.

In this study, we chose the myometrium as an internal reference[27,32] to predict the treatment outcome of HIFU ablation with an immediate NPV ratio of at least 90%. The radiologists manually

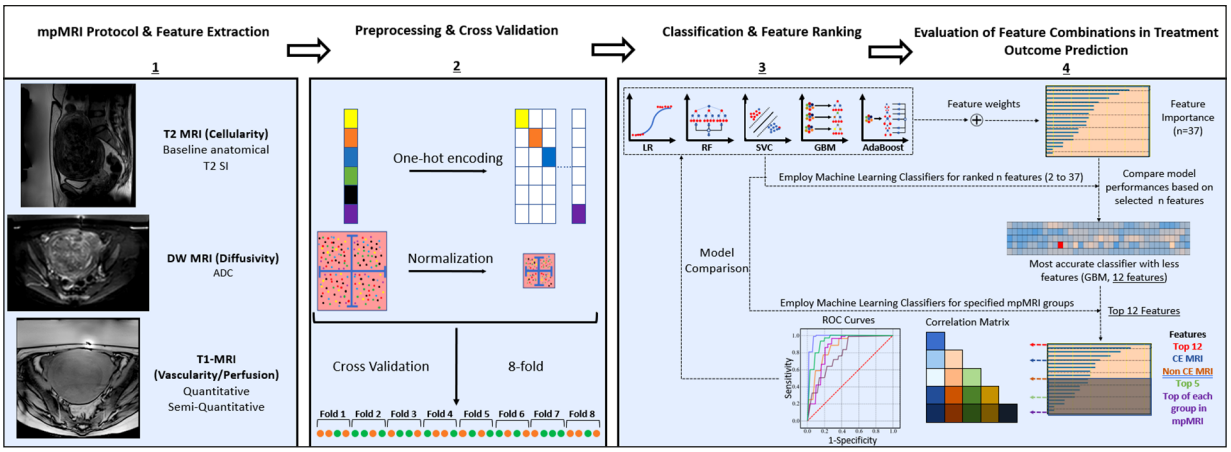

Figure 1. Flowchart of the proposed ML models in predicting the treatment outcome of HIFU ablation with an immediate NPV ratio of at least 90%. (**1**) mpMRI protocol and feature extraction. (**2**) Preprocessing and cross validation. (**3**) Feature ranking and performance evaluation of machine learning algorithms; LR, Logistic regression; SVC, Support vector classifier; RF, Random Forest classifier; GBM, Gradient boosting classifier; AdaBoost, Adaptive boosting classifier. (**4**) Evaluation of feature combinations in treatment outcome prediction.

drew regions of interest (ROIs) on the mpMRI dataset as follows: (1) as large as possible over the center of the uterine fibroids, avoiding the fibroid capsule and the lesion's large vascular supply, and (2) over the myometrium, which includes the maximum area of the smooth muscle tissues avoiding the surrounding structures, lesions, and endometrium.

Preprocessing & Cross-Validation

Following the determination of the categorical values in the data set, these values were converted to numerical values using a hot encoding method. The whole data set of 73 patients was divided into eight groups using 8-fold cross-validation to evaluate the generalizability and accuracy of the model. Seven-folds were set as the training data and the remaining one-fold was set as the test data. Nevertheless, the best-scoring features were selected based on univariate statistical tests inside the cross-validation loop.

Machine Learning Based Feature Ranking and Classifiers

For predicting the treatment outcome of HIFU ablation with an immediate NPV ratio of at least 90% in this study, five ML classifiers – Logistic regression (LR) classifier, Support vector classifier (SVC), Random Forest (RF) classifier, Adaptive boosting (AdaBoost) classifier, and Gradient boosting (GBM) classifier – were used instead of feature selection methods for determining the most important features owing to the following reasons: (1) lack of a specific learning algorithm guiding the feature selection phase in the filter-based feature selection methods, (2) lack of computational efficiency in the wrapper-based methods, and (3) large variation of the performance of the chosen ML classifier algorithm in the embedded-based methods.

Supervised learning algorithms aim to learn the general rules or patterns of the existing training data and data distributions. It is worth noting that although no best algorithm exists in the absolute sense, an algorithm that works best with specific existing research challenges and data can be found according to the prediction performance, stability, and robustness. Therefore, an ensemble feature ranking (EFR) model was introduced based on the score values assigned to the features based on different classifiers to predict the immediate NPV ratio of at least 90%. More specifically, the score values assigned by ML classifiers were summed up and included in the range of [0,1]. The minimum and maximum value from the data was fetched, and each value was replaced according to the following formula.

$$z_i = (b\text{-}a)/(y\text{-}x) * (\text{value } z\text{-}x) + a) \quad (1)$$

where [x, y] and [a, b] represent the range of score values assigned to each feature before and after the normalization condition, and z is the i^{th} normalized data.

Statistical Analysis

Statistical analysis was performed using SPSS software (version 25.0, 64-bit edition, IBM Corp., Armonk, NY, USA). A two-sided *p*-value of <0.05 was considered statistically significant. Continuous variables expressed as mean value ± standard deviation. Chi-square tests or Fischer's exact tests and one-way analysis of variance were employed as considered appropriate. The relationship between the mpMRI features and the immediate NPV ratio of 90% was evaluated using Pearson's correlation coefficients to measure feature importance[33].

The diagnostic ability of ML classifier algorithms was performed using standard performance metrics, including the area under the receiver operating characteristic curve (AUROC), accuracy, sensitivity, and specificity in eight folds cross-validation[34]. The most efficient ML classifiers with the highest AUROC were determined as the predictive model, which was used to predict the treatment outcome of HIFU ablation for uterine fibroids with an immediate NPV ratio of at least 90%.

Results

Feature Ranking

A combination of mpMRI data outlining the anatomical features, and tissue cellularity, diffusivity, and vascularity are essential for analyzing the factors influencing the treatment responsiveness accurately. The mpMRI features were assessed in the following subgroups: (1) anatomical, (2) T2-SI, (3) DW MRI, (4) quantitative perfusion MRI, and (5) semiquantitative perfusion MRI.

The feature rankings for all the 37 features from five different ML classifier algorithms according to the anatomical features and tissue

characteristics were designed to generate the best model to fit the input data and predict the treatment outcome of HIFU ablation with an immediate NPV ratio of at least 90% accurately (Table I).

According to the EFR model and ranking of the importance scores with five ML classifiers (Table II and Figure 2), we included the most informative 12 features suggested by the ML voting system to ensure at least one representative feature of each mpMRI subgroup is included in the analysis. Therefore, as shown in Table II, the most relevant 12 features from highest to lowest ranking were: (1) The K^{trans} ratio of the fibroid to the myometrium, (2) The ratio of the area under the curve (AUC) of the fibroid to the myometrium, (3) Subcutaneous fat thickness, which was measured at the most compressed position, where the distance between the skin and the abdominal wall muscle was the shortest, (4) The ratio of the Maximum Enhancement of the fibroid to the myometrium, (5) K^{trans} value of fibroid, (6) The ratio of Maximum Relative Enhancement of the fibroid to the myometrium, (7) Maximum Enhancement of the fibroid, (8) Anteverted position of the uterus, (9) Time to Peak of the fibroid; (10) The ratio of the ADC value of the fibroid to the myometrium, (11) The ratio of Relative Enhancement of the fibroid to the myometrium, and (12) T2-SI of fibroid.

Characteristics of the MRI Features

No significant intergroup differences were noted among the baseline anatomical features except for subcutaneous fat thickness ($p = 0.0026$, Table III). In the other four subgroups, significant intergroup differences were observed in some mpMRI features (Table IV).

The mean K^{trans} ratio of the fibroid to the myometrium for patients with an NPV ratio of at least 90% and less than 90% was 0.5 ± 0.12 (0.23-0.84) and 1.42 ± 0.72 (0.45-3.19; $p < 0.0001$), respectively. The mean K^{trans} of the uterine fibroids in both the groups, A and B, was 75.3 ± 57.6 (20.1-283.5) and 151.1 ± 97.5 (30.2-292.6; $p < 0.0001$), respectively.

The mean ratio of the AUC of the fibroid to the myometrium of the patients with at least 90% and less than 90% was 0.61 ± 0.22 (0.08-0.98) and 1.12 ± 0.42 (0.14-1.88; $p < 0.0001$), respectively. The mean ratio of the maximum enhancement of the fibroid to the myometrium and the mean ratio of the maximum relative enhancement of the fibroid to the myometrium for patients with an NPV ratio of at least 90% and less than 90% were 0.71 ± 0.24 (0.19-1.25) and 0.65 ± 0.23 (0.13-1.02) and 1.05 ± 0.28 (0.35-1.66; $p < 0.0001$) and 1.12 ± 0.42 (0.31-2.24; $p < 0.0001$), respectively.

The mean relative enhancement ratio, maximum enhancement ratio, and maximum relative enhancement ratio for the patients with an NPV ratio of at least 90% and less than 90%, were 0.71 ± 0.18 (0.37-1.19), 0.71 ± 0.24 (0.19-1.25), and 0.65 ± 0.23 (0.13-1.02), and 1.14 ± 0.45 (0.37-2.29; $p < 0.0001$), 1.05 ± 0.28 (0.35-1.66; $p < 0.0001$), and 1.12 ± 0.42 (0.31-2.24; $p < 0.0001$), respectively. The mean maximum enhancement of the uterine fibroids was 286.9 ± 120.3 (83.3-553.1) for patients with an NPV ratio of at least 90% and 554.4 ± 359.6 (96.8-1750.3; $p < 0.0001$) for the patients with an NPV ratio of less than 90%. The mean time to peak of the uterine fibroids in both the groups, A and B, was 202.7 ± 95.8 (69.3-446.5) and 164.2 ± 51.6 (69.1-284.8; $p = 0.066$), respectively.

The mean ratio of the ADC value of the fibroid to the myometrium for patients with an NPV ratio of at least 90% and less than 90% was 0.66 ± 0.22 (0.25-1.16) and 0.79 ± 0.19 (0.34-1.19; $p = 0.0184$), respectively. The mean T2-SI of the uterine fibroids in both the groups, A and B, was calculated as 75.8 ± 66.0 (19.0-332.0) and 80.7 ± 60.4 (20.0-249.0; $p = 0.76$), respectively.

Tables III and IV summarize the anatomical and baseline characteristics of the study population and tissue characteristics derived from the mpMRI protocol.

Correlation with An Immediate NPV Ratio of at Least 90%

The K^{trans} ratio of the fibroid to the myometrium, one of the quantitative perfusion MRI features, demonstrated the highest negative correlations with an NPV ratio of at least 90% ($r = -0.72$, $p < 0.0001$; Pearson's correlation test). The Pearson's correlation analysis also revealed a significant negative correlation between the K^{trans} of the fibroid and the NPV ratio of at least 90% ($r = -0.44$, $p = 0.0001$).

Among the semiquantitative perfusion MRI features, except time to peak of the fibroid ($r = 0.22$, $p = 0.0656$), all the other features including the ratio of the AUC of the fibroid to the myometrium ($r = -0.63$, $p < 0.0001$), the ratio of the maximum relative enhancement of the fibroid to the myometrium ($r = -0.59$, $p < 0.0001$), the ratio of the relative enhancement of the fibroid to the

Table I. Score values assigned to 37 features by ML classifier algorithms

mpMRI		Parameters	LR	SVC	RF	AdaBoost	GBM	ENSEMBLE
Anatomical		Anteverted	10	11	17	2	11	8
		Retroverted	11	12	29	21	10	16
		Bulk Positive	36	35	32	21	24	37
		Bulk Negative	35	34	23	21	24	36
		Fibroid Diameter	34	36	27	6	23	32
		Intramural	29	24	33	21	24	30
		Submucosal	26	22	15	21	24	27
		Subserosal	21	10	9	13	24	15
		Skin to fibroid distance	27	33	30	2	24	24
		Subcutaneous Fat Thickness	4	2	13	6	22	3
Cellularity	T2SI	Fibroid	23	7	22	6	3	12
		Myometrium	28	26	25	13	13	28
		Fibroid/Myometrium	30	29	16	13	16	29
Diffusivity	ADC	Fibroid	13	14	34	6	17	13
		Myometrium	33	32	24	21	12	35
		Fibroid/Myometrium	12	9	20	13	14	10
Quantitative Perfusion	K^{trans}	Fibroid	2	4	6	21	6	5
		Myometrium	31	13	28	21	9	25
		Fibroid/Myometrium	1	1	1	1	1	1
Semi Quantitative Perfusion	Area Under the Curve	Fibroid	37	30	11	21	24	34
		Myometrium	20	16	26	21	24	23
		Fibroid/Myometrium	3	3	2	21	5	2
	Maximum Enhancement	Fibroid	8	8	4	13	24	7
		Myometrium	16	18	12	21	19	20
		Fibroid/Myometrium	6	5	3	6	8	4
	Maximum Relative Enhancement	Fibroid	14	20	19	21	20	22
		Myometrium	24	31	35	21	24	31
		Fibroid/Myometrium	5	6	5	21	15	6
	Relative Enhancement	Fibroid	15	25	18	13	24	18
		Myometrium	25	37	37	13	24	33
		Fibroid/Myometrium	7	17	7	21	24	11
	Time to Peak	Fibroid	18	15	10	2	21	9
		Myometrium	32	23	36	6	18	26
		Fibroid/Myometrium	22	29	31	6	2	21
	Wash in Rate	Fibroid	19	27	14	2	4	14
		Myometrium	17	21	21	13	7	19
		Fibroid/Myometrium	9	19	8	21	24	17

Table II. An ensemble model by using the score value assigned to the features by the ML classifiers.

Features	RANK
K^{trans}-Fibroid/myometrium	1
Area Under the Curve-Fibroid/Myometrium	2
Subcutaneous Fat Thickness	3
Maximum Enhancement-Fibroid/Myometrium	4
K^{trans}-Fibroid	5
Maximum Relative Enhancement-Fibroid/Myometrium	6
Maximum Enhancement-Fibroid	7
Anteverted	8
Time to Peak-Fibroid	9
ADC-Fibroid/Myometrium	10
Relative Enhancement-Fibroid/Myometrium	11
T2-Fibroid	12
ADC-Fibroid	13
Wash in Rate-Fibroid	14
Subserosal	15
Retroverted	16
Wash in Rate-Fibroid/Myometrium	17
Relative Enhancement-Fibroid	18
Wash in Rate-Myometrium	19
Maximum Enhancement-Myometrium	20
Time to Peak-Fibroid/Myometrium	21
Maximum Relative Enhancement-Fibroid	22
Area Under the Curve-Myometrium	23
Skin to Fibroid Distance	24
K^{trans}-Myometrium	25
Time to Peak-Myometrium	26
Submucosal	27
T2-Myometrium	28
T2-Fibroid/Myometrium	29
Intramural	30
Maximum Relative Enhancement-Myometrium	31
Fibroid Diameter	32
Relative Enhancement-Myometrium	33
AUC-Fibroid	34
ADC-Myometrium	35
Bulk-Negative	36
Bulk-Positive	37

myometrium (r = -0.56, $p < 0.0001$), the ratio of the maximum enhancement of the fibroid to the myometrium (r = -0.53, $p < 0.0001$), and the maximum enhancement of the fibroid (r = -0.47, $p < 0.0001$) had a significant negative correlation with the NPV ratio of at least 90%.

Meanwhile, the ratio of the ADC value of the fibroid to the myometrium (r = -0.28, $p = 0.0184$) and the subcutaneous fat thickness (r = -0.348, $p = 0.0026$) negatively correlated with the NPV ratio of at least 90% (r = -0.28, $p = 0.0184$), while no significant correlation was found between the T2-SI of the fibroid and the NPV ratio of at least 90% (r = -0.037, $p = 0.7585$) and the anteverted position of the uterus and the NPV ratio of at least 90% (r = -0.198, $p = 0.0934$). The pairwise Pearson's correlation coefficients between the most informative 12 features and NPV ratio of at least 90%, and best performing features from each mpMRI group and NPV ratio of at least 90% are shown in Figures 3 and 4, respectively.

Predictive Performance of the Classifiers and the Most Informative mpMRI Features

Figure 5 and Table V show the receiver operating characteristic analyses in 8-fold cross-validation (7 in the training cohort and 1 in the testing cohort), thereby presenting the performance of the five ML classifiers in predicting the treatment outcome of HIFU ablation with an immediate NPV ratio of 90% for the most informative 12 features. In addition, the performance of the same ML classifiers in predicting the treatment out-

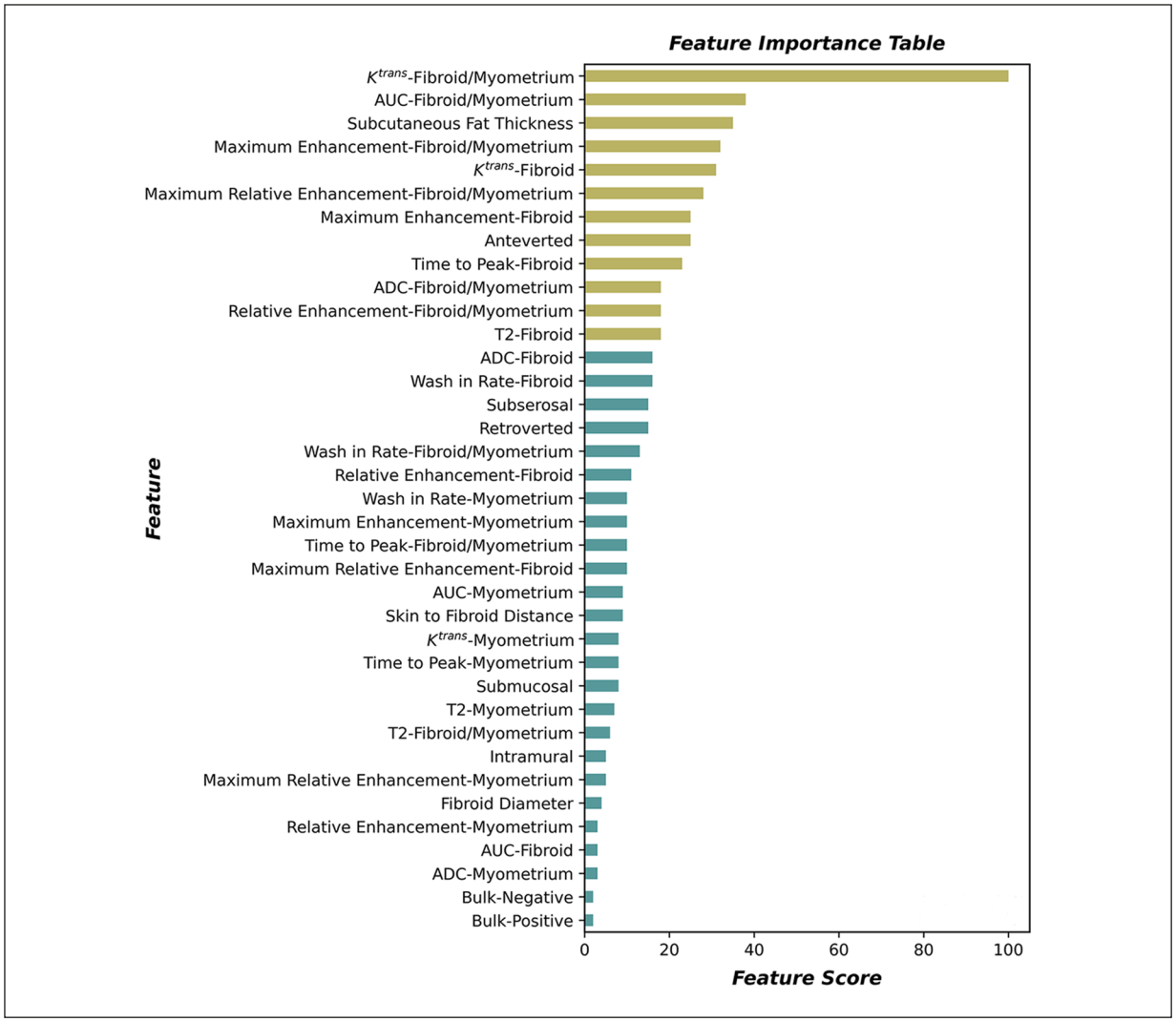

Figure 2. Feature importance of mpMRI model in prediction of treatment outcome of HIFU ablation with an immediate NPV ratio of at least 90%.

Table III. Comparison of anatomical and baseline characteristics according to the NPV ratio of at least 90% and less than 90%.

Anatomical/Baseline features	NPV ≥ 90%	NPV < 90%	*p*
Subcutaneous Fat Thickness (mm)	14.12 ± 4.48 (5-26)	10.6 ± 4.61 (3-25)	0.002
Skin to fibroid distance (mm)	93 ± 17.28 (59-133)	90.79 ± 16.29 (57-127)	0.592
Uterus Position			0.093
Anteverted	20	29	
Retroverted	5	19	
Bulk			0.402
Yes	20	42	
No	5	6	
Fibroid Diameter (mm)	64.12 ± 19.38 (30-97)	66.4 ± 28.45 (24-151)	0.721
Fibroid Type			0.601
Intramural	11	23	
Submucosal	6	14	
Subserosal	8	11	

Table IV. T2 SI, Perfusion and Diffusion Features Derived from the mpMRI protocol According to the NPV Ratio of at Least 90% and Less Than 90%.

mpMRI	Features	All (n = 73)			NPV ≥ 90 (n = 48)			NPV < 90 (n = 25)I		
		Fibroid	Myometrium	Ratio	Fibroid	Myometrium	Ratio	Fibroid	Myometrium	Ratio
T2	T2 SI	77.45 ± 64.08 (19-332)	147.29 ± 124.01 (30-706)	0.62 ± 0.31 (0.16-1.58)	75.77 ± 66 (19-332)	155.52 ± 130 (30-706)	0.57 ± 0.66 (0.16-1.58)	80.68 ± 60.39 (20-249)	131.48 ± 112.16 (34-440)	0.71 ± 0.29 (0.32-1.47)
DWI	ADC	0.97 ± 0.26 (0.32-1.62)	1.42 ± 0.29 (0.64-2.06)	0.71 ± 0.22 (0.25-1.19)	0.93 ± 0.29 (0.32-1.62)	1.44 ± 0.30 (0.92-2.06)	0.66 ± 0.22 (0.25-1.16)	1.05 ± 0.19 (0.6-1.39)	1.39 ± 0.29 (0.64-1.78)	0.79 ± 0.19 (0.34-1.19)
T1-quantitative perfusion	K^{trans}	101.25 ± 81.58 (20.13-392.57)	137.01 ± 83.51 (29.19-489.35)	0.81 ± 0.61 (0.23-3.19)	75.28- ± 57.64 (20.13-283.51)	145.26 ± 84.60 (48.42-489.35)	0.5 ± 0.12 (0.23-0.84)	151.13 ± 97.55 (30.24-392.57)	121.17 ± 80.67 (29.19-325.56)	1.42 ± 0.72 (0.45-3.19)
T1-semi quantitative perfusion	Relative enhancement	99.93 ± 40.91 (32.58-228.57)	122.41 ± 42.53 (37.95-261.11)	0.86 ± 0.36 (0.37-2.29)	89.18 ± 34.53 (32.58-166.43)	125.93-41.59 (47.06-261.11)	0.71 ± 0.18 (0.37-1.19)	120.59 ± 44.85 (43.14-228.57)	115.65 ± 44.34 (37.95-217.91)	1.14 ± 0.45 (0.37-2.29)
	Maximumt enhancemen	375.13 ± 260.18 (83.32-1750.32)	128.82 ± 43.27 (38.15-273.71)	0.83 ± 0.3 (0.19-1.66)	286.95 ± 120.30 (83.32-553.09)	408.22 ± 116.74 (183.53-719.25)	0.71 ± 0.24 (0.19-1.25)	544.45 ± 359.62 (96.83-1750.32)	512.92 ± 288.32 (244-1265.73)	1.05 ± 0.28 (0.35-1.66)
	Maximum Relative enhancement	100.35 ± 45.12 (10.04-221.53)	128.82 ± 43.27 (38.15-273.71)	0.81 ± 0.38 (0.13-2.24)	87.56 ± 39.56 (10.04-153.7)	132.75 ± 42.92 (52.13-273.71)	0.65 ± 0.23 (0.13-1.02)	124.92 ± 45.7 (34.9-221.53)	121.29 ± 43.8 (38.15-215.18)	1.12 ± 0.42 (0.31-2.24)
	Time to peak	189.49 ± 84.93 (69.11-446.51)	178.71 ± 60.8 (69.28-337.17)	1.07 ± 0.36 (0.43-2.58)	202.68 ± 95.78 (69.26-446.51)	178.09 ± 64.65 (69.26-337.17)	1.13 ± 0.37 (0.6-2.58)	164.18 ± 51.56 (69.11-284.8)	179.9 ± 56.16 (101.46-307.68)	0.95 ± 0.31 (0.43-2.07)
	Wash-in rate	17.63 ± 25.94 (0.78-215.72)	18.59 ± 12.65 (3.25-76.23)	0.91 ± 0.62 (0.02-3.25)	10.73 ± 7.60 (0.78-29.83)	16.19 ± 9.69 (3.25-43.49)	0.7 ± 0.29 (0.02-1.24)	30.87 ± 40.34 (2.76-215.72)	23.18 ± 16.21 (5.02-76.23)	1.32 ± 0.85 (0.36-3.25)
	AUC	58545.43 ± 49244.72 (1953.33 -216554.4)	76474.49 ± 64558.95 (8481.95-315522.17)	0.79 ± 0.39 (0.08-1.88)	51793.54 ± 49914.53 (2044.17-21655.4)	81662.79 ± 72170.39 (8481.94-315522.17)	0.61 ± 0.22 (0.08-0.98)	71509.07 ± 46149.55 (1953.33-158292.62)	66512.95 ± 46327.79 (14249.21-160782.4)	1.12 ± 0.42 (0.14-1.88)

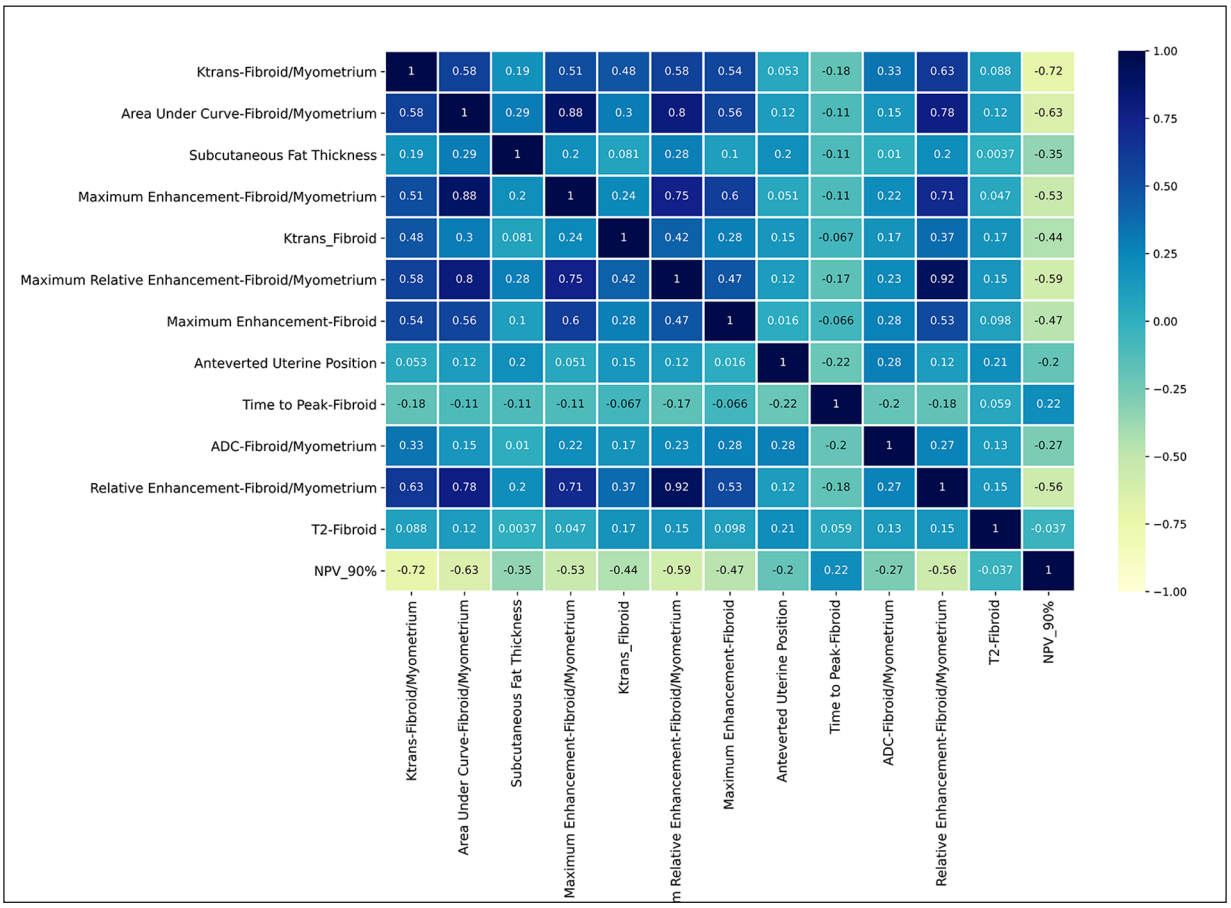

Figure 3. The pairwise Pearson's correlation coefficients among most informative 12 MRI features.

come of HIFU ablation with an immediate NPV ratio of 90% for the best performing features from each mpMRI group is shown in Figure 6 and Table VI.

Furthermore, we have also investigated whether the most informative features extracted from the mpMRI protocol can better predict the treatment outcome of HIFU ablation with an immediate NPV ratio of 90% using the best classifier. Figures 7 and 8 illustrate the performance of the most informative 12 and best performing features from each mpMRI group in predicting the treatment outcome of HIFU ablation with an immediate NPV ratio of 90%, calculated as the best classifier.

Discussion

In general practice, category distinctions and associated tissue responsiveness information are essential for increasing the granularity of data analysis. This is particularly relevant as the majority of uterine fibroids that currently fall in the unsuitable group based on conventional classification could be restratified in the ablation favorable group. Such stratification is dependent on a more in-depth understanding of the factors influencing the treatment outcome. The immediate NPV ratio, one of the key parameters determining therapeutic efficacy, has been proven to be the main factor associated with clinical success. The immediate NPV ratio of MRI-guided HIFU therapy for uterine fibroids was >60% in earlier studies and 90% in recent studies. This value has been set as a measure of technical success[10,13,14,29]. To the best of our knowledge, the present study is the first to combine mpMRI features using ML algorithms to assess the anatomical features and tissue cellularity, diffusivity, and vascularity for predicting the treatment outcome of MRI-guided HIFU ablation with an immediate NPV ratio of at least 90%. Such breakthrough development

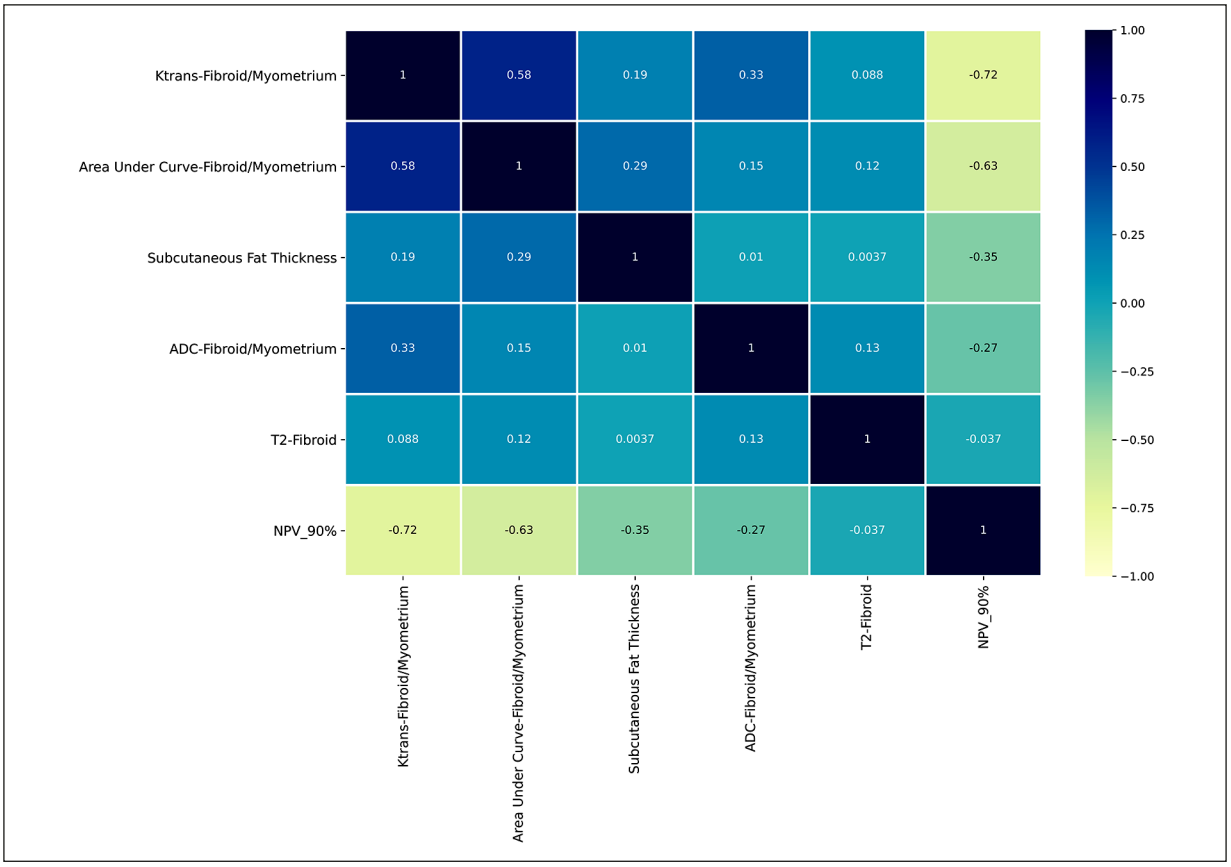

Figure 4. The pairwise Pearson's correlation coefficients among best performing features from each mpMRI group.

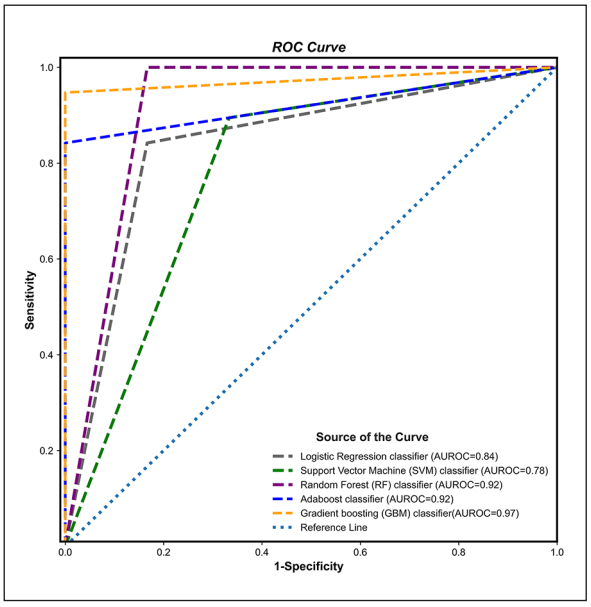

Figure 5. The performance of the five ML techniques in predicting the treatment outcome of high-intensity focused ultrasound (HIFU) ablation with an immediate NPV ratio of 90% for most informative 12 features.

could also remarkably increase the successful application of HIFU ablation and create a higher demand for this treatment as a viable alternative to invasive surgery.

Feature importance scores could be used as the basis for gathering additional or different data. The relative scores could highlight the features that are the most and least important to the ML model when making a prediction. Therefore, by introducing 37 features from the mpMRI data into an EFR model based on the score values assigned to the features by five different ML classifiers, the results of our study presented the 12 most informative and best performing features from each mpMRI group for predicting the immediate HIFU treatment outcome. Using Pearson's correlation analysis, not only the correlation between the 12 most informative mpMRI features with an immediate NPV ratio of at least 90%, but also the correlation among these 12 most informative features were investigated.

One of the most well-established non-invasive imaging techniques that measures tumor per-

Table V. The performance of the five ML techniques in predicting the treatment outcome of HIFU ablation with an immediate NPV ratio of 90% for most informative 12 features.

	Accuracy	Specificity	Sensitivity	AUROC
Logistic regression classifier	0.84	0.83	0.84	0.83
Support vector classifier	0.84	0.66	0.89	0.78
Random forest classifier	0.96	0.83	1	0.92
Adaboost classifier	0.88	1	0.84	0.92
Gradient boosting classifier	0.92	1	0.89	0.95

fusion by providing information on the tumor vascularity, permeability, and blood volume is DCE-MRI, which can be assessed either quantitatively or semiquantitatively. In the present study, the highest-ranking feature for predicting the treatment outcome was the K^{trans} ratio of the fibroid to the myometrium, which is more than twice as important as the rest of the features (Figure 2). The K^{trans} mainly manifests tumor perfusion and vascular permeability. A study by Kim et al[22] suggested that a high K^{trans} value in baseline perfusion MRI is a significant predictor of poor treatment outcomes. Furthermore, Liu et al[24] suggested that K^{trans} maps at the screening phase could aid in visualizing high perfusion areas within the fibroids where sonications should be performed with high therapeutic acoustic power for a better treatment outcome. In our study, the Pearson's correlation analysis showed that both the K^{trans} ratio of the fibroid to the myometrium and the K^{trans} of the fibroid were significant quantitative perfusion MRI features for predicting an NPV ratio of at least 90% (Figure 3). Proper understanding of the strong positive correlation between these two quantitative perfusion MRI features ($r = 0.48$, $p < 0.0001$), and also the strong negative correlation of the same features with an immediate NPV ratio of at least 90% would allow for better patient selection as well as the prescription of a fibroid-specific treatment approach. These findings indicate that a fibroid with significantly higher K^{trans} values in comparison with the normal myometrium shows higher perfusion and rapid blood flow from the surrounding zone where it dissipates the heat accumulation within the fibroid tissue, which may lead to clinical inefficiency in HIFU therapy. Our findings concur with Pennes' equation[35] and the results of previous studies[22-29,31].

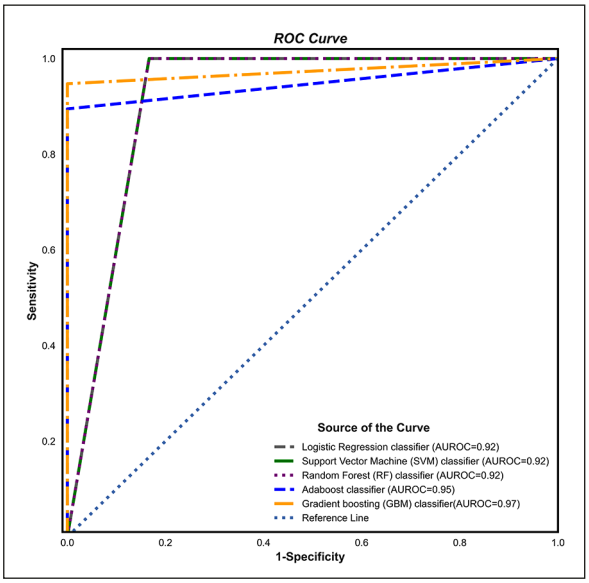

Figure 6. The performance of the five ML techniques in predicting the treatment outcome of HIFU ablation with an immediate NPV ratio of 90% for best performing features from each mpMRI group.

Table VI. The best classifier performance with best performing features from each mpMRI in predicting the treatment outcome of HIFU ablation with an immediate NPV ratio of 90%.

	Accuracy	Specificity	Sensitivity	AUROC
Logistic regression classifier	0.96	0.83	1	0.92
Support vector classifier	0.96	0.83	1	0.92
Random forest classifier	0.96	0.84	1	0.92
Adaboost classifier	0.92	1	0.89	0.95
Gradient boosting classifier	0.96	1	0.84	0.97

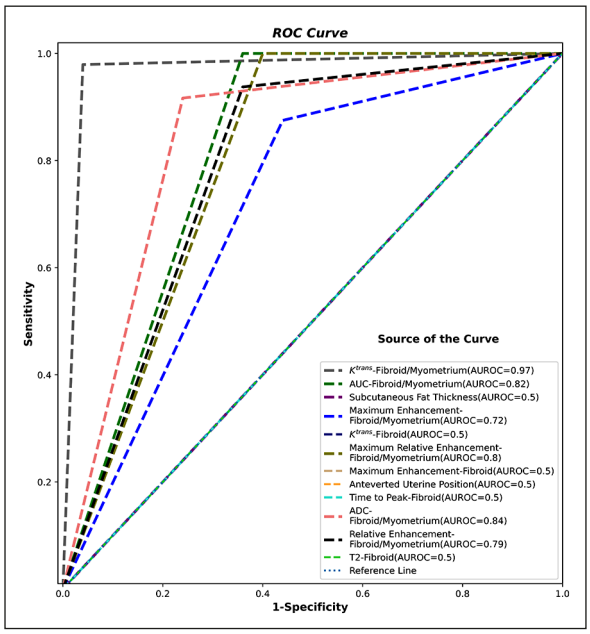

Figure 7. The performance of most informative 12 features in predicting the treatment outcome of HIFU ablation with an immediate NPV ratio of 90%, calculated with GBM Classifier.

As shown in Table II, VI of the 12 most informative features belong to the semiquantitative perfusion MRI group, which represents different vascularity and perfusion spectrum phases within the particular fibroids. The AUC exhibits passage of the entire column of contrast passing through the regional circulatory system at a specific period, thus explaining the spectral phases, which are related to the amount and flow rate of blood circulation, vessel wall permeability, the available interstitial space, and the reabsorption rate. The maximum enhancement of the fibroids provides information about the maximum vascularity and perfusion of the fibroid. High values indicate a higher blood delivery and increased leakage to the extracellular space, which leads to increased total gadolinium concentration within that particular fibroid. The current study demonstrated that the fibroid tissue, in the group with an NPV ratio of less than 90%, has a steep rise and more intense enhancement in the early phase of the time-SI curve, followed by a plateau in the late phase. A steep rise in the time-SI curve reflects its fast perfusion rate, while intense enhancement indicates high gadolinium concentration owing to increased delivery by the dense capillary network. On the contrary, fibroid tissue, in the group with an NPV ratio of at least 90%, has a gradual rise and less intense enhancement, followed by a plateau, indicating a slower filling rate and lesser blood volume passing through its vascular network compared to the normal myometrium.

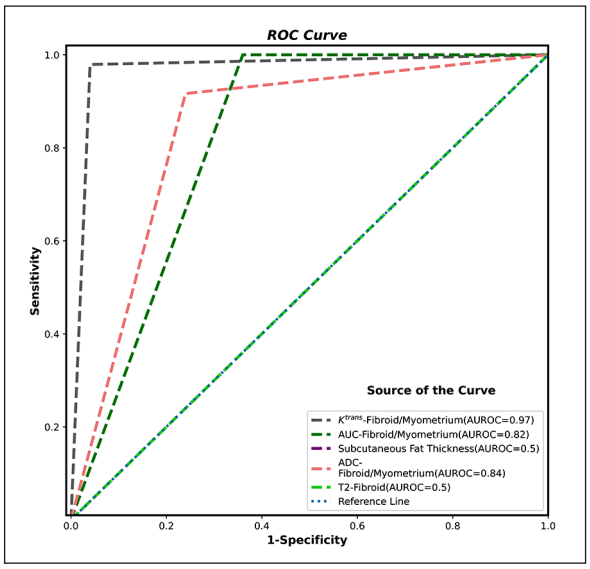

Figure 8. The performance of best performing features from each mpMRI group in predicting the treatment outcome of HIFU ablation with an immediate NPV ratio of 90%, calculated with GBM Classifier.

Of the six semiquantitative perfusion MRI features, significant negative correlations were noted between the five features (all except time to peak of fibroid) with an immediate NPV ratio of at least 90% and significant positive correlations among these same five features as follow: between (i) the ratio of the AUC of the fibroid to the myometrium and the ratio of the maximum enhancement of the fibroid to the myometrium ($r = 0.88$, $p < 0.0001$), (ii) the ratio of the AUC of the fibroid to the myometrium and the ratio of the maximum relative enhancement of the fibroid to the myometrium ($r = 0.8$, $p < 0.0001$), (iii) the ratio of the AUC of the fibroid to the myometrium and the ratio of the relative enhancement of the fibroid to the myometrium ($r = 0.78$, $p < 0.0001$), (iv) the ratio of the AUC of the fibroid to the myometrium and the maximum enhancement of the fibroid ($r = 0.56$, $p < 0.0001$), (v) the ratio of the maximum enhancement of the fibroid to the myometrium and the ratio of the relative enhancement of the fibroid to the myometrium ($r = 0.71$, $p < 0.0001$), (vi) the ratio of the maximum enhancement of the fibroid to the myometrium and the maximum enhancement of the fibroid ($r = 0.6$, $p < 0.0001$), (vii)

the ratio of the maximum enhancement of the fibroid to the myometrium and the ratio of the maximum relative enhancement of the fibroid to the myometrium (r = 0.75, $p < 0.0001$), (viii) the ratio of the maximum relative enhancement of the fibroid to the myometrium and the ratio of the relative enhancement of the fibroid to the myometrium (r = 0.92, $p < 0.0001$), (ix) the ratio of the maximum relative enhancement of the fibroid to the myometrium and the maximum enhancement of the fibroid (r = 0.47, $p < 0.0001$), and (x) the maximum enhancement of the fibroid and the ratio of the relative enhancement of the fibroid to the myometrium (r = 0.53, $p < 0.0001$). These correlations highlight the essential role of the vascularity in achieving a higher treatment success rate. Tissues with higher perfusion tend to have less effective energy deposition owing to the fast blood inflow within the tissue and fast clearance of heat via the capillary and venous networks, which also reduces accumulation of the heating energy that is considered essential to meet the ablation temperature requirement needed for effective treatment. More sonication using higher energy is needed in such fibroids to reach the effective ablation temperature. Moreover, maintaining the temperature level could be challenging owing to increased blood circulation turnover within these fibroids. As mentioned above, the blood flow velocity correlates positively with the degree of heat drain and influences the heat accumulation within the tissue. These findings are consistent with those of previous studies[23,25,29,30].

DW imaging is influenced by a range of parameters, including cellular membrane integrity, extracellular fluid viscosity, cellularity, and tissue vascularity. It assesses the random movement of water molecules in each tissue voxel and represents diffusion in the intracellular, extracellular, or in between them. In contrast, ADC quantifies the molecular diffusion of water (tissue diffusion) and the microcirculation of blood in the capillaries (perfusion). Since fibroids comprise varying ratios of smooth muscle cells and fibrous connective tissue, although the intracellular diffusion is similar among fibroids in different groups, the extracellular space varies resulting in the difference in diffusivity. It is worth noting that fibroids with low cellularity have a relative increase in the extracellular space, allowing free water diffusion, whereas water diffusion is restricted in highly cellular fibroids owing to reduced extracellular space. The present study shows that the ratio of the ADC value of the fibroid to the myometrium was the tenth best ranking feature overall and the most informative diffusion feature in predicting the treatment outcome of HIFU ablation with an NPV ratio of at least 90% (r = -0.275, $p = 0.0184$). This indicates that fibroids with lower ADC values, demonstrating hypercellularity, have a better treatment response than hypocellular fibroids with substantially higher ADC values. HIFU thermally ablates the fibroid cells, thereby explaining the higher success rates in hypercellular tumors. Moreover, there is a significant positive correlation between the ratio of the ADC value of the fibroid to the myometrium with three perfusion MRI features: K^{trans} ratio of the fibroid to the myometrium (r = 0.334, $p = 0.0039$), the ratio of the maximum relative enhancement of the fibroid to the myometrium (r = 0.227, $p = 0.0539$) and the maximum enhancement of the fibroid (r = 0.277, $p = 0.0176$). This suggests that the patients with a low ADC and perfusion value would have better ablation results than those with merely a low value in either component. These findings indicate that the ratio of the ADC value of the fibroid to the myometrium is another beneficial feature that should be included in the MRI screening protocol to improve the post-HIFU treatment success rate. These results are in line with previous research findings in the following studies by Ikink et al[17], Sainio et al[21], and Andrews et al[31].

The use of HIFU in the treatment of uterine fibroids has improved significantly since the introduction and adaptation of the T2 SI-based classification system in 2007 as a standard classification system[5]. Fibroids with different SIs on T2W MRI have a significant influence on the treatment outcome attributed to the differences in water content, tissue density, and cellular arrangement. Previous studies have demonstrated that uterine fibroids with high T2W SI have a higher ratio of smooth muscle to collagen fibers, which is the best-known "resistant to tissue heating" feature[5,10,15,25,29,32,36]. More specifically, higher SI on T2W MRI of uterine fibroids indicates the presence of angiogenesis and an abundance of cellular components with less water and fibrous tissue. In contrast, fibroids with lower SI on T2W MRI have lesser angiogenesis and more abundant fibrous content. In addition, fibroids with higher water content and lower density have a lower heating effect owing to reduced acoustic impedance secondary to their

low density. It also has reduced acoustic attenuation coefficients owing to higher moisture within. Zhao et al[12] emphasized the importance of cellularity using *in vitro* HIFU ablation. The fibroids with a higher SI in this study have a lesser necrotic region post-HIFU ablation and vice versa. This study protocol has eliminated the effect of perfusion on fibroid ablation, an essential compounding factor as mentioned earlier. Our study demonstrates that the T2-SI of the fibroid is the least important ranking feature overall among the 12 most informative mpMRI features; however, it is the most informative cellularity feature. It had no significant correlation with the NPV ratio of at least 90% and the rest of 12 most informative features. However, the T2-SI ratio of the fibroid to the myometrium had a significant positive correlation with both the K^{trans} ratio of the fibroid to myometrium (r = 0.313, $p = 0.007$) and the ratio of the AUC of the fibroid to myometrium (r = 0.316, $p = 0.0065$). Such correlations could explain the synergistic nature of perfusion and cellularity in more accurately and reliably identifying the responsiveness to HIFU ablation.

Previous studies[10,12,23,29] have demonstrated that a thick subcutaneous adipose tissue would absorb more acoustic energy and induce an increase in skin temperature, potentially leading to tissue damage, primarily in the subcutaneous tissue. In contrast, a thin subcutaneous adipose tissue, together with anterior sonications, would increase skin heating and the likelihood of skin burns. Kim et al[22] demonstrated that the thickness of the subcutaneous adipose tissue was one of the significant anatomical parameters influencing the HIFU ablation of uterine fibroids. A recent study by Keserci et al[29] proved that the thickness of the subcutaneous adipose tissue in the anterior abdominal wall was a valuable predictor of the outcome of HIFU ablation when the NPV ratio was at least 90%. In addition, the thickness of the subcutaneous adipose tissue was ranked second among the 10 highest-ranking features reported by Suomi et al[16]. In the current study, there was a significant negative correlation between the subcutaneous fat thickness, the third-best ranking feature overall and the most informative anatomical feature, and an NPV ratio of at least 90% (r = -0.348, $p = 0.0026$). This negative correlation could be owing to the effect of the thick subcutaneous adipose tissue in the abdominal wall, which causes wave distortion or increased absorption of acoustic energy leading to heat accumulation in the near field of the ultrasonic beam path. Such a condition increases the risk of fat burn and affects the beam focus quality, thus limiting the degree of tissue ablation in HIFU treatment of uterine fibroids. The fat thickness also has a significant positive correlation with the ratio of the AUC of the fibroid to the myometrium (r = 0.292, $p = 0.0123$) and the ratio of the maximum relative enhancement of the fibroid to the myometrium (r = 0.284, $p = 0.0149$) in the NPV ratio of at least 90% group. A fast enhancement rate and increased perfusion compounded the effect of reduced effective heating caused by the large subcutaneous fat layer leading to an increased insufficient thermal dose delivery effect in the hypervascular fibroid tissue in this group of patients, as seen in the NPV ratio of less than 90% group.

In our study, the anteverted position of the uterus was the second most important anatomical feature. A previous study also reported that patients with anterior fibroids, higher SI on T2W MRI of uterine fibroids, and an anteverted position of the uterus had a higher NPV ratio[37]. This could be explained by the shorter distance that the ultrasound wave had to penetrate in the acoustic pathway of the patients with the anteverted uterus position, thus allowing more acoustic energy deposition at the targeted fibroids. Therefore, more heat is deposited within the fibroid, thereby allowing a higher NPV value immediately post-HIFU treatment. Sonication can also be delivered at a higher power with a longer duration owing to a relatively acceptable distance from the vital structures and nerves in the anteverted location. This is consistent with the findings published by Zhao et al[12], Fan et al[37], Zhang et al[38], and Keserci et al[39]. Furthermore, there is a positive correlation between the anteverted position of the uterus and the ADC ratio of the fibroid to the myometrium. This indicates that fibroids with lower ADC values would achieve a higher NPV value in patients with an anteverted position of the uterus than in retroverted ones.

The AUROC curves presented in this study allow the clinician to estimate the probability of a patient achieving an NPV ratio of at least 90% in HIFU treatment of uterine fibroids. Choosing a cutoff value for predicting an NPV ratio of at least 90% is challenging owing to the implicit trade-offs between sensitivity and specificity. Thus, the EFR model and ranking of importance scores with five ML classifier algorithms would either introduce

eligible patients with high confidence of achieving an NPV ratio of at least 90% or rule out the patients who have a lower chance of achieving an NPV ratio of at least 90%. The GBM classifier, which is more robust against outliers and has high computational power, showed the best predictive performance with an AUROC of 0.95 and accuracy of 0.92, followed by the RF, AdaBoost, LR, and SVC classifiers, which yielded an AUROC of 0.92, 0.92, 0.83 and 0.78, and accuracy of 0.96, 0.88, 0.84 and 0.84, respectively (Table V). The best classifier performance with the best performing features from each mpMRI group (Table VI), K^{trans} ratio of the fibroid to the myometrium, the ratio of the AUC of the fibroid to the myometrium, subcutaneous fat thickness, the ratio of ADC value of the fibroid to the myometrium, and T2-SI of fibroid, was achieved using GBM whose AUROC and accuracy values were 0.97 and 0.96, followed by AdaBoost (AUROC=0.94, accuracy=0.92), RF (AUROC=0.92, accuracy=0.96), SVC (AUROC=0.91, accuracy=0.96) and LR classifiers (AUROC=0.92, accuracy=0.96). The K^{trans} ratio of the fibroid to the myometrium had the highest AUROC (0.97), followed by the ratio of the ADC value of fibroid to the myometrium (0.83), the ratio of the AUROC of the fibroid to the myometrium (0.82), the ratio of the maximum relative enhancement of the fibroid to the myometrium (0.8), the ratio of the relative enhancement of the fibroid to the myometrium (0.79), the ratio of the maximum enhancement of the fibroid to the myometrium (0.72), K^{trans} of the fibroid (0.5), maximum enhancement of the fibroid (0.5), subcutaneous fat thickness (0.5), T2-SI of the fibroid (0.5), anteverted position of the uterus (0.5), and time to peak of the fibroid (0.5). For all the 12 most informative features, the AUROC ranged from 0.5 to 0.97, accuracy ranged from 0.34 to 0.97, specificity ranged from 0.56 to 1.0, and sensitivity ranged from 0.87 to 1.0. These findings are promising and suggest that the use of these features could be an excellent reference when attempting to predict the treatment outcome of HIFU ablation with an immediate NPV ratio of 90% in clinical practice.

This study has some limitations. First, it was a single-center study with a relatively small sample size. Therefore, a lack of validation data from the different mpMRI protocols for generalization could be present. Further multicenter studies are warranted for large-scale evaluation and validation of the role of the mpMRI features in predicting the treatment outcome of HIFU ablation of uterine fibroids with an immediate NPV ratio of at least 90%. Secondly, ADC maps were calculated using the combination of b-values of 0, 200, 400, 600, and 800 s/mm^2 in this study, which reflect a combination of diffusion and perfusion effects. Future studies must include intravoxel incoherent motion-DW MRI, including pseudo-diffusion coefficient (D*), tissue-diffusion coefficient (D), and perfusion fraction (f), with a larger number of low b-values (<200) to simultaneously quantify the diffusion of water molecules and microcirculation perfusion in uterine fibroids. These features could be helpful in patient selection for HIFU treatment of uterine fibroids and predicting treatment outcomes even in the early stage. Similarly, quantitative perfusion MRI features, such as the rate constant between the extravascular extracellular space and blood plasma (Kep), Extravascular Volume fraction (Ve), and Plasma Volume fraction (Vp) also need to be collected and analyzed to provide a more holistic assessment of the perfusion effect. Such features were not assessed in this study owing to limited software availability and short study duration. Third, in this study, the ROI encompassing the largest fibroid was manually drawn upon screening T2W, perfusion MR images over the center of the fibroid using delineation on the center slice of T2W MRI, T1W perfusion MRI, and autogenerated ADC map. This could have attributed to the limitations in reflecting the overall content of the fibroid and adequately describing its heterogeneity. Principally, assessment of the whole-tumor ROI should provide more representative information on tissue cellularity, vascularity, and diffusivity. Considering the potential inhomogeneity of fibroid tumors, such assessment seems to be particularly important for the evaluation of HIFU ablation efficacy in future studies. Moreover, we used myometrium as the internal reference for the fibroid for the comparison with normal parenchyma, as this is a common practice when describing a lesion as seen in cases of hepatocellular carcinoma or renal tumors. Since the myometrium also possesses progressive continuous enhancement post gadolinium, it can be used to differentiate different fibroid types due to differences in the enhancement patterns.

Conclusions

The preliminary findings in this study indicate that gynecologists and radiologists should consider the 12 most informative and best performing

features from each mpMRI group while predicting the treatment outcome of HIFU ablation to achieve an immediate NPV ratio of 90%, which was defined as a measure of clinical treatment success. The main aim of our study was to create a breakthrough in the use and interpretation of tissue cellularity, vascularity, and diffusivity through ML-based novel models using advanced mpMRI data and to correlate significant features with the outcome of HIFU treatment ablation in the screening phase, thereby providing a viable alternative to surgery.

Conflict of Interest
The Authors declare that they have no conflict of interests.

Data Availability
The datasets generated and/or analyzed during the current study are not publicly available due to privacy concerns but are available from the corresponding author on reasonable request.

Authors' Contribution
E. Akpinar and O.-C Bayrak; Coding, data analysis and co-writing the paper. M.-D. Nguyen, C. Nadarajan, M.-H Müslümanoğlu; Data collection, data analysis and interpretation, and revisions to scientific content of manuscript. B. Keserci; Supervising the research, Design of the study, data analysis and interpretation, writing the paper and revisions to scientific content of manuscript.

Funding
This work was supported by The Scientific and Technological Research Council of Türkiye (TUBITAK) [2232-118C221].

Ethical Statement
The institutional review board of Pham Ngoc Thach University of Medicine approved this retrospective study.

Informed Consent
Due to the retrospective nature of this study, the requirement for informed consent was waived by institutional review board of Pham Ngoc Thach University of Medicine.

References

1) Marshall LM, Spiegelman D, Barbieri RL, Goldman MB, Manson JE, Colditz GA, Willett WC, Hunter DJ. Variation in the incidence of uterine leiomyoma among premenopausal women by age and race. Obstet Gynecol 1997; 90: 967-973.
2) Baird DD, Dunson DB, Hill MC, Cousins D, Schectman JM. High cumulative incidence of uterine leiomyoma in black and white women: ultrasound evidence. Am J Obstet Gynecol 2003; 188: 100-107.
3) Marsh EE, Ekpo GE, Cardozo ER, Brocks M, Dune T, Cohen LS. Racial differences in fibroid prevalence and ultrasound findings in asymptomatic young women (18-30 years old): a pilot study. Fertil Steril 2013; 99: 1951-1957.
4) Evans P, Brunsell S. Uterine fibroid tumors: diagnosis and treatment. Am Fam Phys 2007; 75: 1503-1508.
5) Funaki K, Fukunishi H, Funaki T, Sawada K, Kaji Y, Maruo T. Magnetic resonance-guided focused ultrasound surgery for uterine fibroids: relationship between the therapeutic effects and signal intensity of preexisting T2-weighted magnetic resonance images. Am J Obstet Gynecol 2007; 196: 184.e1-6.
6) Stewart EA, Gostout B, Rabinovici J, Kim HS, Regan L, Tempany CM. Sustained relief of leiomyoma symptoms by using focused ultrasound surgery. Obstet Gynecol 2007; 110: 279-287.
7) Arleo EK, Khilnani NM, Ng A, Min RJ. Features influencing patient selection for fibroid treatment with magnetic resonance-guided focused ultrasound. J Vasc Interv Radiol 2007; 18: 681-685.
8) Fennessy FM, Tempany CM, McDannold NJ, So MJ, Hesley G, Gostout B, Kim HS, Holland GA, Sarti DA, Hynynen K, Jolesz FA, Stewart EA. Uterine leiomyomas: MR imaging-guided focused ultrasound surgery--results of different treatment protocols. Radiology 2007; 243: 885-893.
9) Lénárd ZM, McDannold NJ, Fennessy FM, Stewart EA, Jolesz FA, Hynynen K, Tempany CM. Uterine leiomyomas: MR imaging-guided focused ultrasound surgery--imaging predictors of success. Radiology 2008; 249: 187-194.
10) Mikami K, Murakami T, Okada A, Osuga K, Tomoda K, Nakamura H. Magnetic resonance imaging-guided focused ultrasound ablation of uterine fibroids: early clinical experience. Radiat Med 2008; 26: 198-205.
11) Morita Y, Ito N, Hikida H, Takeuchi S, Nakamura K, Ohashi H. Non-invasive magnetic resonance imaging-guided focused ultrasound treatment for uterine fibroids - early experience. Eur J Obstet Gynecol Reprod Biol 2008; 139: 199-203.
12) Zhao WP, Chen JY, Zhang L, Li Q, Qin J, Peng S, Li KQ, Wang ZB, Chen WZ. Feasibility of ultrasound-guided high intensity focused ultrasound ablating uterine fibroids with hyperintense on T2-weighted MR imaging. Eur J Radiol 2013; 82: e43-9.
13) Park MJ, Kim YS, Rhim H, Lim HK. Safety and therapeutic efficacy of complete or near-complete ablation of symptomatic uterine fibroid tumors by MR imaging-guided high-intensity focused US therapy. J Vasc Interv Radiol 2014; 25: 231-239.

14) Mindjuk I, Trumm CG, Herzog P, Stahl R, Matzko M. MRI predictors of clinical success in MR-guided focused ultrasound (MRgFUS) treatments of uterine fibroids: results from a single centre. Eur Radiol 2015; 25: 1317-1328.

15) Zhao WP, Chen JY, Chen WZ. Effect of biological characteristics of different types of uterine fibroids, as assessed with T2-weighted magnetic resonance imaging, on ultrasound-guided high intensity focused ultrasound ablation. Ultrasound Med Biol. 2015; 41: 423-431.

16) Suomi V, Komar G, Sainio T, Joronen K, Perheentupa A, Blanco Sequeiros R. Comprehensive feature selection for classifying the treatment outcome of high-intensity ultrasound therapy in uterine fibroids. Sci Rep 2019; 9: 10907.

17) Gong C, Lin Z, Lv F, Zhang L, Wang Z. Magnetic resonance imaging parameters in predicting the ablative efficiency of high-intensity focused ultrasound for uterine fibroids. Int J Hyperthermia 2021; 38: 523-531.

18) Jacobs MA, Herskovits EH, Kim HS. Uterine fibroids: diffusion-weighted MR imaging for monitoring therapy with focused ultrasound surgery--preliminary study. Radiology 2005; 236: 196-203.

19) Jacobs MA, Gultekin DH, Kim HS. Comparison between diffusion-weighted imaging, T2-weighted, and postcontrast T1-weighted imaging after MR-guided, high intensity, focused ultrasound treatment of uterine leiomyomata: preliminary results. Med Phys 2010; 37: 4768-4776.

20) Ikink ME, Voogt MJ, van den Bosch MA, Nijenhuis RJ, Keserci B, Kim YS, Vincken KL, Bartels LW. Diffusion-weighted magnetic resonance imaging using different b-value combinations for the evaluation of treatment results after volumetric MR-guided high-intensity focused ultrasound ablation of uterine fibroids. Eur Radiol 2014; 24: 2118-2127.

21) Sainio T, Saunavaara J, Komar G, Mattila S, Otonkoski S, Joronen K, Perheentupa A, Blanco Sequeiros R. Feasibility of apparent diffusion coefficient in predicting the technical outcome of MR-guided high-intensity focused ultrasound treatment of uterine fibroids - a comparison with the Funaki classification. Int J Hyperthermia 2021; 38: 85-94.

22) Kim YS, Lim HK, Kim JH, Rhim H, Park BK, Keserci B, Köhler MO, Bae DS, Kim BG, Lee JW, Kim TJ, Sokka S, Lee JH. Dynamic contrast-enhanced magnetic resonance imaging predicts immediate therapeutic response of magnetic resonance-guided high-intensity focused ultrasound ablation of symptomatic uterine fibroids. Invest Radiol 2011; 46: 639-647.

23) Kim YS, Kim BG, Rhim H, Bae DS, Lee JW, Kim TJ, Choi CH, Lee YY, Lim HK. Uterine fibroids: semiquantitative perfusion MR imaging pa¬rameters associated with the intra-procedural and immediate postprocedural treatment effi¬ciencies of MR imaging-guided high-intensity focused ultrasound ablation. Radiology 2014; 273: 462-471.

24) Liu J, Keserci B, Yang X, Wei J, Rong R, Zhu Y, Wang X. Volume transfer constant (Ktrans) maps from dynamic con¬trast enhanced MRI as potential guidance for MR-guided high intensity focused ultrasound treatment of hypervascular uterine fibroids. Magn Reson Imaging 2014; 32: 1156-1161.

25) Kim YS, Lee JW, Choi CH, Kim BG, Bae DS, Rhim H, Lim HK. Uterine Fibroids: Correlation of T2 Signal Intensity with Semiquantitative Perfusion MR Parameters in Patients Screened for MR-guided High-Intensity Focused Ultrasound Ablation. Radiology 2016; 278: 925-935.

26) Kim YS, Lim HK, Park MJ, Rhim H, Jung SH, Sohn I, Kim TJ, Keserci B. Screening magnetic resonance imaging-based prediction model for assessing immediate therapeutic response to magnetic resonance imaging-guided high-intensity focused ultrasound ablation of uterine fibroids. Invest Radiol 2016; 51: 15-24.

27) Keserci B, Nguyen D. The role of T1 perfu¬sion-based classification in magnetic reso¬nance-guided high-intensity focused ultra¬sound ablation of uterine fibroids. Eur Radiol 2017; 27: 5299-5308.

28) Wei C, Fang X, Wang CB, Chen Y, Xu X, Dong JN. The predictive value of quantitative DCE metrics for immediate therapeutic response of high-intensity focused ultrasound ablation (HIFU) of symptomatic uterine fibroids. Abdom Radiol (NY) 2018; 43: 2169-2175.

29) Keserci B, Nguyen D. Magnetic resonance im¬aging parameters in predicting the treatment outcome of high-intensity focused ultrasound ablation of uterine fibroids with an immediate nonperfused volume ratio of at least 90%. Acad Radiol 2018; 25: 1257-1269.

30) Wang YJ, Zhang PH, Zhang R, An PL. Predictive Value of Quantitative Uterine Fibroid Perfusion Parameters From Contrast-Enhanced Ultrasound for the Therapeutic Effect of High-Intensity Focused Ultrasound Ablation. J Ultrasound Med 2019; 38: 1511-1517.

31) Andrews S, Yuan Q, Bailey A, Xi Y, Chopra R, Staruch R, Pedrosa I. Multiparametric MRI Characterization of Funaki Types of Uterine Fibroids Considered for MR-Guided High-Intensity Focused Ultrasound (MR-HIFU) Therapy. Acad Radiol 2019; 26: e9-e17.

32) Lin CN, Liao YS, Chen WC, Wang YS, Lee LW. Use of Myometrium as an Internal Reference for Endometrial and Cervical Cancer on Multiphase Contrast-Enhanced MRI. PLoS One 2016; 11: e0157820.

33) Spearman C. The proof and measurement of association between two things. By C. Spearman, 1904. Am J Psychol 1987; 100: 441-471.

34) Fawcett T. An Introduction to ROC Analysis. Pattern Recognition Letters 2006; 27: 861-874.

35) Pennes HH. Analysis of tissue and arterial blood temperatures in the resting human forearm. J Appl Physiol 1948; 1: 93-122.

36) Ueda H, Togashi K, Konishi I, Kataoka ML, Koyama T, Fujiwara T, Kobayashi H, Fujii S, Konishi J. Unusual appearances of uterine leiomyomas: MR imaging findings and their histopathologic backgrounds. Radiographics 1999; 19: S131-145.

37) Fan HJ, Cun JP, Zhao W, Huang JQ, Yi GF, Yao RH, Gao BL, Li XH. Factors affecting effects of ultrasound guided high intensity focused ultrasound for single uterine fibroids: a retrospective analysis. Int J Hyperthermia 2018; 35: 534-540.

38) Zhang W, He M, Huang G, He J. A comparison of ultrasound-guided high intensity focused ultrasound for the treatment of uterine fibroids in patients with an anteverted uterus and a retroverted uterus. Int J Hyperthermia 2016; 32: 623-629.

39) Keserci B, Duc NM, Nadarajan C, Huy HQ, Saizan A, Wan Ahmed WA, Osman K, Abdullah MS. Volumetric MRI-guided, high-intensity focused ultrasound ablation of uterine leiomyomas: ASEAN preliminary experience. Diagn Interv Radiol 2020; 26: 207-215.